GEOPHYSICS, VOL. 80, NO. 2 (MARCH-APRIL 2015); P. D161–D173, 6 FIGS., 2 TABLES.
10.1190/GEO2014-0368.1

Permeability prediction based on induced polarization: Insights from measurements on sandstone and unconsolidated samples spanning a wide permeability range

Andreas Weller[1], Lee Slater[2], Andrew Binley[3], Sven Nordsiek[4], and Shujie Xu[3]

ABSTRACT

We have compared various induced polarization (IP) models for permeability prediction of the same general form that were all based on two parameters, the first being an electric substitute of effective porosity (the formation factor) and the second being an electric proxy of pore-normalized surface area (the imaginary part of electric conductivity). These models (empirically derived and based on mechanistic formulations) were applied to an extensive database acquired on sandstones and unconsolidated sandy materials. Whereas previous studies on permeability prediction mainly concentrated on either sandstone or unconsolidated sediments, we investigated a database composed of 94 samples including sandstones and unconsolidated material. Most of the samples in the database were saturated with a NaCl solution with an electric conductivity close to 100 mS/m. Samples with a saturating fluid that deviated from this composition were corrected using recently published relationships describing the IP dependence on the pore fluid composition. In the case of the sandstone samples, the electric formation factor exerts the primary control on permeability, and the imaginary conductivity was found to be of little importance in permeability prediction. The opposite was observed for the unconsolidated samples, in which the imaginary conductivity was the most important term for permeability and the formation factor was found to be of little importance. The findings suggest that only one property (formation factor in the case of sandstone, imaginary conductivity in the case of unconsolidated samples) might be needed for the order of magnitude estimates of permeability from the popular form of the model based on the IP observations examined here. Whereas the formation factor was challenging to reliably estimate in situ, the imaginary conductivity was directly obtainable from an IP measurement. This suggests that field scale, single-frequency, IP-based estimation of permeability would be challenging, and possibly ineffective, in sandstones.

INTRODUCTION

Geoelectric measurements are widely applied for hydrogeologic investigations. They provide structural information on the depth and extent of aquifers and aquicludes. Geoelectric measurements also provide opportunities to predict petrophysical parameters of the geologic units, one of the most valuable being permeability k because it determines the resistance of a porous material to fluid flow. Porosity and surface area (inversely related to pore size) are often the key parameters controlling permeability. There have been several studies to relate permeability to the direct current (DC) electric conductivity of porous materials (see, e.g., Slater, 2007). However, no universal trend between permeability and DC electric conductivity can exist. This is a consequence of the DC electric conductivity of a rock being controlled by two conduction mechanisms: (1) electrolytic conduction in the pore fluid filling the interconnected pores and (2) surface conductivity in the electric double layer (EDL) at the boundary between the mineral constituents and the fluid. The electrolytic conduction depends on the electric conduc-

Manuscript received by the Editor 8 August 2014; revised manuscript received 6 November 2014; published online 27 February 2015.
[1]Technische Universität Clausthal, Institut für Geophysik, Clausthal-Zellerfeld, Germany. E-mail: andreas.weller@tu-clasuthal.de.
[2]Rutgers-Newark, Department of Earth and Environmental Sciences, New Jersey, USA. E-mail: lslater@andromeda.rutgers.edu.
[3]Lancaster University, Lancaster Environment Centre, Lancaster, UK. E-mail: a.binley@lancaster.ac.uk; joyceyxus@gmail.com.
[4]Technische Universität Braunschweig, Institut für Geophysik und extraterrestrische Physik, Braunschweig, Germany. E-mail: s.nordsiek@tu-braunschweig.de.

tivity of the pore fluid and the interconnected porosity. The surface conductivity is related to the specific internal surface that increases with decreasing pore or grain size. As a result, a positive correlation between electric conductivity and hydraulic conductivity will exist due to the mutual positive dependence of both properties on porosity in coarse-grained soils with relatively high electrolyte conductivity where surface conduction is small (Heigold et al., 1979; Mazac and Landa, 1979; Frohlich et al., 1996; Purvance and Andricevic, 2000). In contrast, the permeability will decrease with increasing electric conductivity when surface conductivity variations, associated with changes in the concentration of the fine fraction (silt and clay), exert a dominant control on electric conductivity (Kelly, 1977; Kosinski and Kelly, 1981; Urish, 1981; Ponzini et al., 1983; Kelly and Reiter, 1984; Purvance and Andricevic, 2000). Therefore, it is not possible to extract information on the variations in porosity (controlling factor on electrolytic conduction) and variations in grain size (controlling factor on surface conduction) from a single resistivity measurement.

Induced polarization (IP) measurements provide the opportunity to resolve this ambiguity and improve the reliability of permeability prediction from geoelectric measurements (Börner et al., 1996; Slater and Lesmes, 2002; Slater, 2007; Revil and Florsch, 2010). The IP data can be acquired in conjunction with resistivity measurements using time- or frequency-domain IP instrumentation. It is now well recognized that IP measurements are primarily controlled by the lithological properties of the rock (e.g., Börner and Schön, 1991; Börner et al., 1996). More specifically, IP measurements directly sense the polarization of the mineral-fluid interface and are primarily related to the surface conductivity and surface area of the interconnected pore network. Electric models to describe IP data have evolved to use a complex surface conductivity term, where the real part of the surface conductivity represents electromigration of charge along the mineral-fluid interface and the imaginary part represents the polarization of charge at the mineral-fluid interface (e.g., Vinegar and Waxman, 1984; Lesmes and Frye, 2001; Revil and Florsch, 2010). Former studies demonstrate strong relationships between (1) the imaginary part of conductivity and surface conductivity (e.g., Vinegar and Waxman, 1984; Börner et al., 1996; Revil, 2012; Weller et al., 2013) and (2) the imaginary part of conductivity and the surface area normalized to the pore volume (e.g., Börner et al., 1996; Weller et al., 2010b; Revil, 2012). As previously discussed, the surface conductivity and specific internal surface are related to the pore size required to predict permeability.

In this study, we compare models for permeability prediction that are all based on two parameters. In each case, one of these parameters is related to porosity ϕ and the second parameter is related to the pore-normalized surface area. We compare models using an extensive database acquired on sandstones and unconsolidated sandy materials that originate from different labs. The models we consider are empirically derived (e.g., Rink and Schopper, 1974; Slater and Lesmes, 2002) and based on mechanistic formulations (e.g., Revil and Florsch, 2010; Revil, 2012). Several studies have evaluated the applicability of different existing models of permeability prediction at the field scale or in the laboratory (e.g., Slater, 2007; Hördt et al., 2009; Attwa and Günther, 2013; Weller et al., 2014).

The findings of our present study yield new insights into the potential to estimate permeability from IP measurements and the relative importance of porosity and effective pore size in determining permeability of sandstone versus unconsolidated samples.

ELECTRIC PROPERTIES

Measurements

The electric properties of rocks, including conduction and polarization effects, can be concisely represented by a complex conductivity $\sigma*$, which is expressed in terms of magnitude $|\sigma|$ and phase φ or by real (σ') and imaginary (σ'') components:

$$\sigma^* = |\sigma| \cdot e^{i\varphi} = \sigma' + i\sigma'', \tag{1}$$

with $i = \sqrt{-1}$ being the imaginary unit. Generally, the complex electric conductivity of earth materials is frequency dependent $\sigma^*(\omega)$, where the angular frequency ω is related to the measured frequency f by $\omega = 2\pi f$.

Spectral IP (SIP) measurements provide additional information beyond that obtained from a single-frequency IP measurement. SIP measurements are typically made over a frequency range from as low as 10^{-3} to 10^{3} Hz.

Relaxation models can be used to concisely represent the shape of the complex conductivity dependence on frequency in terms of a small number of parameters. Nordsiek and Weller (2008) formulate a Debye decomposition (DD) approach to concisely represent the measured frequency-dependent complex conductivity of a sample. In this approach, $\sigma^*(\omega)$ is represented by a superposition of n Debye relaxation models:

$$\sigma^*(\omega) = \sigma_0 / \left(1 - \sum_{j=1}^{n} m_j \times \left(1 - \frac{1}{1 + i\omega\tau_j}\right)\right), \tag{2}$$

with m_j and τ_j being the chargeability and relaxation-time parameters of a single relaxation term. Decomposition of the spectra into several Debye models results in a distribution of relaxation times, which can be summarized by four integrating parameters. The first parameter is the conductivity σ_0 obtained from extrapolation of the amplitude spectra to low frequency.

According to the original definition of chargeability m given by Sumner (1976),

$$m = \frac{\sigma_\infty - \sigma_0}{\sigma_\infty}, \tag{3}$$

where σ_∞ is the high-frequency asymptotic value of conductivity. When applied over the limited frequency range of measurements, the chargeability quantifies the relative change of conductivity over the frequency scan. The polarization magnitude m_j computed for each individual Debye relaxation term, therefore, specifies the conductivity change over a narrow frequency interval. The summation across the measured frequency range yields a global term, defined here as total chargeability

$$m_t = \sum_{j=1}^{n} m_j, \tag{4}$$

being the second integrating parameter of a DD. Multiplication of the total chargeability m_t, and low-frequency conductivity σ_0 gives the normalized chargeability

$$m_n = m_t \sigma_0. \tag{5}$$

The normalized chargeability m_n represents a polarization magnitude similar to imaginary conductivity except that it is weighted by the observed frequency dependence. The third and fourth integrating parameters of the DD are the mean relaxation time and the degree of uniformity (Nordsiek and Weller, 2008). For the sake of brevity, these last two parameters are not discussed further here because they are not used in our analysis of the k models.

Revil et al. (2014a) propose that a decomposition based on a Debye-type model is physically unrealistic when considering the polarization of a sand grain. They argue that the decomposition should in fact be performed with a Warburg model, and they demonstrate significant differences between the distribution of relaxation times for the DD versus the Warburg decomposition, with the latter providing better consistency with the independently measured distribution of pore sizes. Given that our analysis only uses the global polarization magnitude determined from the decomposition and does not consider the predicted distribution of relaxation times, application of a Warburg model in the decomposition has not been considered here for the sake of brevity.

Models

Most models for the complex electric conductivity of a porous material at low frequencies (e.g., less than 100 Hz) are based on a parallel addition of two conduction terms representing (1) an electrolytic contribution via conduction through the interconnected pore space (σ_{el}) and (2) a mineral surface contribution via conduction and polarization within the EDL of the interconnected pore surface (σ^*_{surf}) (e.g., Vinegar and Waxman, 1984)

$$\sigma^* = \sigma_{el} + \sigma^*_{surf}. \tag{6}$$

The assumption that polarization is only associated with the surface conductivity is valid at the low frequencies (<1 kHz) used in SIP measurements. For a fully saturated medium

$$\sigma' = \frac{1}{F}\sigma_w + \sigma'_{surf}, \tag{7}$$

and

$$\sigma'' = \sigma''_{surf}, \tag{8}$$

where F is the electric formation factor. Archie's law is commonly used to represent F in terms of the interconnected porosity ϕ

$$F = \phi^{-m}, \tag{9}$$

where m is the cementation exponent.

Empirical and mechanistic formulations for surface conductivity exist but are not as well established as Archie's law. These formulations describe the surface conductivity in terms of (1) the volume-normalized surface area or the cation exchange capacity and (2) factors such as the surface charge density and surface charge mobility (Waxman and Smits, 1968; Rink and Schopper, 1974; Vinegar and Waxman, 1984; Weller et al., 2010b; Revil and Skold, 2011). Multiple studies (e.g., Börner et al., 1996; Weller et al., 2010b) have shown that the specific internal surface S_{por} is linearly related to the imaginary part of conductivity σ'' determined by a single-frequency measurement of complex conductivity and the normalized chargeability m_n defined from a DD of frequency-dependent measurements. Weller et al. (2011) introduce the concept of specific polarizability to represent the control of the surface chemistry (e.g., charge density and mobility) on a linear relationship between σ'' and S_{por} observed for an extensive database of sandstone and unconsolidated sediment samples.

RELATIONS BETWEEN ELECTRIC PROPERTIES AND PERMEABILITY

The simplest models of permeability prediction are based on bundles of uniform capillaries that pervade a solid medium. Based on geometric considerations and considering the Hagen-Poiseuille equation, permeability can be determined by the geometric quantities porosity ϕ, pore radius r, and tortuosity T according to the following equation:

$$k = \frac{r^2\phi}{8T}. \tag{10}$$

A variety of models have been proposed to predict permeability from geoelectric measurements. The ratio T/ϕ can be replaced by the formation factor F (e.g., Guéguen and Palciauskas, 1994, p. 193), if the electric tortuosity is assumed to equal the hydraulic tortuosity. Using $2/S_{por}$ as an equivalent for the capillary radius r, the Kozeny-Carman equation can be formulated

$$k_{KC} = \frac{1}{2FS^2_{por}}, \tag{11}$$

to relate permeability to measurable petrophysical quantities. More rigorous models for permeability prediction have been proposed, for example, based on the electric geometrical parameter Λ (Johnson et al., 1986), which is a weighted pore volume to pore surface ratio with the weight favoring constricted regions of the pore space (i.e., the pore throats). However, SIP models of k estimation primarily evolved from the recognition of the opportunity to substitute proxy measures of F and S_{por} in equation 11, as we review below.

The applicability of equation 11 is restricted to a model of cylindrical capillaries with a smooth surface. The roughness of the internal surface of sandstones, which is well resolved by the nitrogen-adsorption method, requires a modification of equation 11. Considering the fractal nature of the internal surface of sedimentary rocks, Pape et al. (1987) propose the following equation for permeability prediction:

$$k_{PaRiS} = \frac{a_{PaRiS}}{FS^{3.1}_{por}}, \tag{12}$$

which is the so-called PaRiS model. The numerical value of factor a_{PaRiS} is equal to 475 if the permeability is given in 10^{-15} m^2 and the specific internal surface is in $1/\mu$m. The formation factor F is a parameter that is determined from electric measurements, but S_{por} is a geometric quantity that is usually measured by the nitrogen-adsorption method. Binley et al. (2005) find an empirical fit of their set of 17 shaly sandstone samples with an expression that is close to the PaRiS model. The exponent S_{por} empirically derived from their measurements is 3.6, slightly higher than the theoretically derived value of 3.1. Sen et al. (1990) find a similar permeability prediction equation for their set of more than 100 clay-bearing

sandstone samples. However, their exponent of S_{por} is determined to be 2.08, i.e., lower than the exponent of the original PaRiS model.

Prior to the realization that IP could be used to determine surface conductivity and specific surface area, formulae for permeability prediction have been proposed based on the formation factor and surface conductivity determined from multisalinity experiments using geoelectric equipment that only measures conductivity amplitudes (Rink and Schopper, 1974). In this approach, samples were fully saturated with a brine of gradually increasing conductivity. The relationship between sample conductivity and fluid conductivity as described in equation 7 was used to determine F and σ_{surf} from the multisalinity data. Rink and Schopper (1974) investigate 75 samples (mainly sandstones) at eight different salinities. They find an empirical relation for permeability prediction:

$$k_{RS} = \frac{a_{RS}}{F^5 \sigma_{surf}^2}, \tag{13}$$

with a_{RS} being a fitting constant. A similar equation is developed by Revil et al. (2014b) on the basis of a mechanistic model. Using an extensive database, Weller et al. (2013) show that the surface conductivity is linearly related to the imaginary part of conductivity that is directly determined from a complex conductivity measurement. Consequently, σ_{surf} in equation 13 can be approximated by the imaginary part of conductivity σ'' scaled by a constant representing the slope of the relationship between σ'' and σ_{surf}. This has major implications for geoelectric investigations because the surface conductivity in equation 7 requires laborious, time-consuming multisalinity measurements that could never be performed in the field whereas, in contrast, imaginary conductivity at a single salinity is recorded in laboratory or field geoelectric surveys with an IP instrument. The relatively weak (compared with the electrolytic contribution) dependence of the imaginary conductivity on salinity may still need to be considered (e.g., Revil and Florsch, 2010; Weller et al., 2013).

Based on a mechanistic model, Revil and Florsch (2010) propose a similar equation for permeability prediction of granular media that directly combines the imaginary part of conductivity σ'' and the formation factor F:

$$k_{RF} = \frac{a_{RF}}{F^3 \sigma''^2}, \tag{14}$$

where $F \gg 1$ and the cementation exponent $m = 1.5$. The factor $a_{RF} = (\Sigma^s)^2/4.5$ is related to the specific surface conductivity of the Stern layer Σ^s.

Considering the proportionality between the parameters S_{por}, σ_{surf}, and σ'', we represent them by a common parameter s, leading to a standardized representation of all these equations by

$$k* = \frac{a}{F^b s^c}. \tag{15}$$

Examining equations 11–14, significant variations in the exponents b and c of equation 15 are observed. The exponent b of the formation factor varies between one and five. The exponent c of the parameter s varies between two and 3.6 based on equations 11–14.

Equations 11–14 have been primarily applied to experimental data acquired on sandstone samples. However, Slater and Lesmes (2002) investigate the validity of such permeability prediction models for unconsolidated materials. Considering the weak variation in formation factor (only a factor of three), they do not find any statistical influence of F on the estimated k for their data set. They identify a direct relation between k and the imaginary part of conductivity. Their model can also be described by equation 15 with $b = 0$ and $c = 1.1$.

Beside the class of models of permeability prediction that we focus on in this study, additional models that integrate the time constants of different relaxation models (e.g., the Cole-Cole model) into permeability estimation have been proposed (e.g., Binley et al., 2005; Revil and Florsch, 2010; Zisser et al., 2010). Most of these models are restricted to complex electric conductivity spectra with a distinct phase maximum and require the acquisition of SIP data over a wide frequency range. The resulting time constant is related to a dominant length scale (grain size or pore size) that controls permeability. Our experience is that a relatively small subset of samples is characterized by complex conductivity spectra with a distinct phase peak that can be reliably fitted by relaxation models to yield a time constant (21 out of 56 samples in this study). Furthermore, many samples we have investigated are characterized by measurements over a limited frequency interval and do not show any significant phase peak. The time constants are poorly constrained by the data, and the applicability of models based on time constants is therefore limited.

The DD permits determination of characteristic parameters even of SIP spectra that do not show a distinct phase peak. Weller et al. (2010a) and Zisser et al. (2010) apply the DD approach to spectra of sandstone samples and estimate the permeability by integrating the median and the mean of the resulting relaxation time distribution, respectively. Nevertheless, it often remains impractical to reliably acquire SIP data over a wide frequency range in the field, whereas the acquisition of single-frequency IP data, or IP data over a limited low-frequency range, is more straightforward. Similarly, although borehole tools are available to acquire measures of the polarization magnitude in well logging, no such tools for acquiring SIP data required to determine the relaxation time distribution currently exist. Consequently, the approach to permeability prediction based on a measured time constant is very challenging beyond the laboratory, and we are unaware of any published work in which this has been achieved. In contrast, field-scale estimation of permeability from measures of the polarization magnitude has been reported in several studies. Consequently, we focus our paper on samples characterized by such data sets.

SAMPLES, MEASUREMENTS, AND PROCESSING

Our primary database is made up of 56 sandstone samples and 22 samples of unconsolidated sandy material with available complex conductivity spectra $\sigma^*(\omega)$, formation factors, and permeability values that originate from multiple sources (Flath, 1989; Lesmes and Frye, 2001; Slater and Glaser, 2003; Breede, 2006; Schröder, 2008; Revil et al., 2013, Weller et al., 2013, Slater et al., 2014; Zhang and Weller, 2014) and hitherto unpublished studies. In all cases, we had access to the original data. All samples were saturated with a reference sodium chloride solution of approximately 0.5 g/l resulting in a predefined fluid conductivity of $\sigma_f \approx 100$ mS/m. The references, permeability, formation factor, imaginary conductivity, normalized chargeability, and a description of the sandstone samples are compiled in Table 1. The details of the unconsolidated samples are summarized in Table 2.

Table 1. Summary of the 56 sandstone samples used in this study, showing permeability k, formation factor F, fluid conductivity σ_w, imaginary part of conductivity at 1 Hz σ'', normalized chargeability m_n, sample description, and source of original data.

Sample	k (m^2)	F	σ_w (mS/m)	σ'' at 1 Hz (mS/m)	m_n (mS/m)	Description
			Flath (1989)			
H18H	5.76E – 14	18.6	111.7	0.6187	2.510	Sherwood
H18V	4.16E – 14	17.1	111.0	0.6350	2.624	Sherwood
H46H1	7.15E – 13	12.9	111.7	0.5370	2.165	Sherwood
H46V1	1.57E – 12	11.5	113.2	0.5116	2.036	Sherwood
H62H1	6.43E – 13	13.8	112.3	0.3827	1.599	Sherwood
H62V1	1.41E – 13	14.8	111.0	0.4000	1.619	Sherwood
HCF120H	7.75E – 15	29.1	111.4	0.6475	2.986	Sherwood
HCF120V	5.80E – 16	44.1	112.1	0.4654	2.200	Sherwood
HCF197H1	1.23E – 12	12.8	111.9	0.8178	3.036	Sherwood
HCF197V1	2.48E – 13	11.8	113.2	0.6821	2.556	Sherwood
HCF233H	2.61E – 13	18.0	110.8	0.8167	3.388	Sherwood
HCF233V1	5.27E – 15	28.1	110.4	0.7314	3.245	Sherwood
HCF236H1	2.11E – 13	18.6	112.3	0.7654	3.338	Sherwood
HCF236V	1.35E – 13	17.7	111.7	0.7083	2.966	Sherwood
P19H	7.06E – 13	13.3	112.8	0.7887	2.773	Sherwood
P19V1	7.74E – 13	12.9	113.8	0.8062	2.863	Sherwood
P39H1	4.45E – 13	13.0	111.7	0.9342	3.533	Sherwood
P39V1	2.37E – 13	12.1	111.2	0.8747	3.065	Sherwood
P40H1	3.38E – 13	15.9	112.1	1.0260	3.897	Sherwood
P40V1	8.34E – 14	17.4	113.6	1.0056	3.664	Sherwood
P53H1	1.53E – 13	11.9	111.7	0.9777	4.969	Sherwood
P56V	3.48E – 14	15.7	111.2	0.7609	4.616	Sherwood
P68H1	3.16E – 13	15.9	112.8	0.9860	4.316	Sherwood
P68V	2.37E – 13	13.1	113.8	1.0731	4.769	Sherwood
			Lesmes and Frye (2001)			
B-LF	2.28E – 13	16.7	128.4	0.0876	0.711	Berea
			Breede (2006)			
GR	3.30E – 13	11.7	92.0	0.2910	1.365	Greensand
BU3	2.00E – 17	68.4	91.7	0.1796	0.756	Bunter
BU12	3.41E – 13	17.6	96.2	0.0536	0.314	Bunter
BK	1.97E – 12	18.2	96.0	0.0429	0.240	Helsby
BS4	4.23E – 13	17.8	101.4	0.1615	0.846	Kiddminster
BR5	4.65E – 12	9.0	95.1	0.2709	1.314	Helsby
			Schröder (2008)			
BU1	1.91E – 16	38.0	90.0	0.3344	1.496	Bunter
OK4	7.39E – 15	24.8	90.0	0.1123	0.591	Obernkirchener
B49H	6.85E – 14	26.8	90.0	0.0295	0.174	Bahariya
B49V	4.75E – 14	31.0	90.0	0.0295	0.169	Bahariya
B4H	3.00E – 16	44.9	90.0	0.0538	0.321	Bahariya
B4V	2.40E – 16	59.6	90.0	0.0388	0.215	Bahariya
GR1	1.98E – 12	9.4	90.0	0.2931	1.391	Greensand
			Zhang and Weller (2014)			
CS-11	6.24E – 16	37.1	96.4	0.2776	1.641	Shahejie
CS-13	7.05E – 15	31.7	96.7	0.2647	1.343	Shahejie

Table 1. (continued)

Sample	k (m^2)	F	σ_w (mS/m)	σ'' at 1 Hz (mS/m)	m_n (mS/m)	Description
CS-16	9.01E − 15	32.6	98.6	0.1639	0.782	Shahejie
CS-22	4.58E − 17	80.6	98.6	0.0570	0.324	Shahejie
			New samples, this study			
AC5	5.00E − 17	115.7	116.0	0.1550	0.846	Arizona Chocolate
B4	2.15E − 13	15.2	116.0	0.1065	0.735	Berea
BE1	2.50E − 13	22.4	116.0	0.0899	0.534	Bentheimer
BH6-A2	4.27E − 13	14.0	98.6	0.0529	0.360	Bentheimer
CLASH	5.23E − 13	14.4	116.0	0.0945	0.655	Clashach
Co7	2.63E − 15	48.1	116.0	0.1977	1.037	Coconino
E3	4.64E − 12	15.2	116.0	0.0426	0.316	Elb
ES4-R2	2.58E − 13	16.3	102.0	0.3288	2.194	Elb
F5-2	1.50E − 16	151.4	98.6	0.0022	0.019	Fontainebleau
G4	5.73E − 15	27.6	116.0	0.1635	1.122	Gravenhorster
IR01	1.33E − 14	37.8	116.0	0.0418	0.305	Island Rust
IR02	2.23E − 14	33.9	116.0	0.0396	0.292	Island Rust
O5	5.05E − 14	17.5	116.0	0.1327	0.829	Obernkirchener
OK5-R3	4.12E − 14	28.6	100.9	0.1232	0.713	Obernkirchener

We extended this primary database with three additional sets of unconsolidated materials that did not satisfy our stringent requirements regarding σ_f of the saturating fluid. The first set contains six samples from the study of Slater and Glaser (2003) that were saturated with a sodium chloride brine of $\sigma_w = 57$ mS/m. The second set consists of artificial mixtures with different contents of sand, clay, and gravel documented in Xu (2014). The samples of this study were saturated with a sodium chloride brine with the fluid conductivity varying between 55 and 60 mS/m. Because the reference fluid conductivity in our study is $\sigma_f = 100$ mS/m, a correction of σ_0 and σ'' for fluid conductivity variation is necessary (Weller et al., 2011; Weller and Slater, 2012). Assuming a fixed formation factor and ignoring surface conduction, σ_0 can be corrected to the reference fluid conductivity by

$$\sigma_0(\sigma_f) = \frac{\sigma_f}{\sigma_w}\sigma_0(\sigma_w). \tag{16}$$

Surface conduction could be accounted for using a correction procedure proposed in Weller et al. (2013), but this was considered unnecessary for this study. Considering the weaker salinity dependence of the imaginary part of conductivity (Weller et al., 2011), a similar correction can be applied for the imaginary part of conductivity:

$$\sigma''(\sigma_f) = C_f\sqrt{\frac{\sigma_f}{\sigma_w}}\sigma''(\sigma_w), \tag{17}$$

with $C_f = 1$ for the sodium chloride solution.

The third set of additional unconsolidated samples comes from a study in which three natural soil samples (STO, GGL, and VRD) were saturated with a calcium chloride solution of varying water conductivity from 69 to 106 mS/m (Nordsiek et al., 2013). The low-frequency conductivity and the imaginary part of conductivity were corrected according to equations 16 and 17, respectively. Experimental data suggest that the imaginary part of conductivity is approximately halved if a calcium chloride solution is used instead of a sodium chloride brine (Weller et al., 2011), suggesting that an additional correction factor $C_f = 2$ should be used in equation 17 to double the imaginary part of conductivity if a calcium chloride solution is used. Formation factors are not available for the samples STO, GGL, and VRD because the electric measurements were made at low salinity only.

Although the individual data sets are restricted in permeability variation when considered alone, the compiled set of samples covers a wide range in permeability. The permeability of the sandstone samples varies between 2×10^{-17} m^2 and 5×10^{-12} m^2. The permeability of the samples of unconsolidated material ranges from 5×10^{-15} m^2 to 1.7×10^{-10} m^2. Thus, the complete sample set covers a range of seven orders of magnitude. In contrast, previous studies of k estimation using IP data have included at best three–five orders of magnitude of k.

The formation factor F for 42 samples was determined from multisalinity experiments using equation 7. If multisalinity experiments to high salinities were not done, the formation factor F was determined using a single high-conductivity saturating fluid ($\sigma_w > 6$ S/m), and it was assumed that the surface conductivity in equation 7 could be ignored. The estimated formation factor varies between 4 and 15 for the unconsolidated samples and between 9 and 151 for the sandstone samples.

The complex conductivity spectra were obtained by measuring the impedance magnitude and phase shift of the voltage waveform recorded across the sample relative to the current waveform recorded on a reference resistor, the source typically being a sine signal swept over a range of frequencies (e.g., Slater and Lesmes, 2002). All measurements reported here were recorded using a four-electrode setup, whereby separate electrode pairs were used to inject the current into the sample and record the resulting potential waveform across the sample. Measured magnitude and phase

Table 2. Summary of the 38 unconsolidated samples used in this study, showing permeability k, formation factor F, fluid conductivity σ_w, imaginary part of conductivity at 1 Hz σ'', normalized chargeability m_n, sample description, and source of original data.

Sample	k (m^2)	F	σ_w (mS/m)	σ'' at 1 Hz (mS/m)	m_n (mS/m)	Description
			Slater and Glaser (2003)			
N1 26.5–35	5.06E − 12	5.25	130.0	0.0741	0.5270	Sand/silt floodplain sediments
N1 51–53	8.38E − 11	5.46	131.0	0.0303	0.2123	Sand/silt floodplain sediments
N2 27–35	7.65E − 12	4.00	131.0	0.0766	0.5485	Sand/silt floodplain sediments
N2 45–47	1.10E − 10	7.32	114.7	0.0198	0.1261	Sand/silt floodplain sediments
N2 47–55	7.08E − 11	5.30	124.6	0.0413	0.3170	Sand/silt floodplain sediments
N1 22.5–25	2.17E − 12	2.93	57.0	0.0250	0.1617	Sand/silt floodplain sediments
N1 37–40	9.90E − 12	5.59	57.0	0.0277	0.2736	Sand/silt floodplain sediments
N1 44–51	1.69E − 11	3.43	57.0	0.0110	0.0840	Sand/silt floodplain sediments
N2 19–25	8.38E − 12	4.89	57.0	0.0653	0.4489	Sand/silt floodplain sediments
N2 25–26.5	1.64E − 12	4.49	57.0	0.0367	0.3063	Sand/silt floodplain sediments
N2 55–60	2.75E − 11	8.66	57.0	0.0147	0.1022	Sand/silt floodplain sediments
			Revil et al. (2013)			
S9	1.60E − 14	4.10	121.0	0.6610	5.0817	Saprolite
S16	5.00E − 15	5.90	121.0	0.7960	5.0932	Saprolite
S22	7.70E − 15	4.40	122.0	1.6300	11.8808	Saprolite
			Weller et al. (2013)			
2_21c47_48	4.87E − 11	12.59	118.9	0.0484	0.3611	Sand and gravel flood deposits
2_19c50_51	5.38E − 11	9.05	87.8	0.0499	0.4214	Sand and gravel flood deposits
2_24c42_43	6.12E − 11	9.94	108.9	0.0494	0.3683	Sand and gravel flood deposits
			Slater et al. (2014)			
B1_47.65–49	3.23E − 11	12.53	100.0	0.0148	0.1071	Sands and gravels
B2,4, 35–36.45	6.88E − 11	9.50	100.0	0.0081	0.0550	Sands and gravels
B3_2_14.8–16	4.39E − 11	12.29	100.0	0.0167	0.1143	Sands and gravels
B4_7_54–55.2	6.28E − 11	10.49	100.0	0.0209	0.1399	Sands and gravels
B6_7_52.95–54	2.79E − 11	13.01	100.0	0.0340	0.2133	Sands and gravels
C1_5_43.95–45	2.20E − 11	12.77	100.0	0.0236	0.1677	Sands and gravels
C2_7_52–53.8	2.47E − 11	14.62	100.0	0.0153	0.0962	Sands and gravels
C3_5_34.45–36	3.22E − 11	13.92	100.0	0.0153	0.1099	Sands and gravels
C3_3_17.05–18	3.63E − 11	8.20	100.0	0.0186	0.1400	Sands and gravels
C4,2_10.25–12.0	6.57E − 11	4.90	100.0	0.0375	0.2368	Sands and gravels
C5,5 34–46	5.77E − 11	10.65	100.0	0.0184	0.1111	Sands and gravels
			Xu (2014)			
100%s	7.40E − 11	5.18	54.7	0.0183	0.1485	Sand
99%s1%c	6.52E − 11	4.02	58.7	0.0322	0.2287	Sand-clay-mixture
95%s5%cA	8.15E − 12	3.66	60.3	0.0664	0.6957	Sand-clay-mixture
90%s10%c	3.78E − 13	5.82	54.7	0.1400	1.2085	Sand-clay-mixture
70%s30%c	1.27E − 13	4.99	59.0	0.4090	3.1631	Sand-clay-mixture
70%s30%g	1.68E − 10	6.29	60.0	0.0157	0.1336	Sand-gravel-mixture
60%s10%c30%g	1.40E − 13	8.22	56.6	0.1430	1.2151	Sand-clay-gravel
			Nordsiek et al. (2013)			
STO	4.64E − 12	Not determined	69.0	0.0157	0.1611	Sandy soil
GGL	8.61E − 13	Not determined	101.3	0.1140	0.9128	Loamy soil
VRD	1.94E − 13	Not determined	105.8	0.0893	0.5921	Loamy soil

were converted into a complex conductivity (σ^*) using the geometric factor defining the measurement geometry and the current flow path (assumed 1D) in the test device.

For this analysis, we focus on the imaginary part of conductivity σ'' at a frequency of approximately 1 Hz. This is somewhat arbitrary, although it is representative of the frequencies usually measured with time-domain IP instruments, and is at the frequency most commonly used to analyze IP data in the reported literature. However, considering a single frequency neglects any information contained in the shape of the phase spectrum. This additional information might be expected to improve permeability prediction because the shape of the spectrum is typically considered to result from the grain or pore size distribution (Lesmes and Morgan, 2001; Revil and Florsch, 2010). The normalized chargeability m_n was, therefore, also calculated from equation 5 using the fitting parameters of the DD.

The data from all investigated samples were used to determine the free parameters (the factor a, and the two exponents b and c) in the different versions of equation 15 by multiple regression. In addition to the coefficient of determination R^2 of the fitting equation, the average absolute deviation (in log space) between predicted permeability k^* and measured permeability k

$$d = \frac{1}{n}\sum_{j=1}^{n} |\log_{10}(k_j) - \log_{10}(k_j^*)|, \tag{18}$$

was used for a quantitative evaluation of the predictive quality of the different models. A value of $d = 1$ denotes an average absolute deviation of one order of magnitude (or a factor of 10).

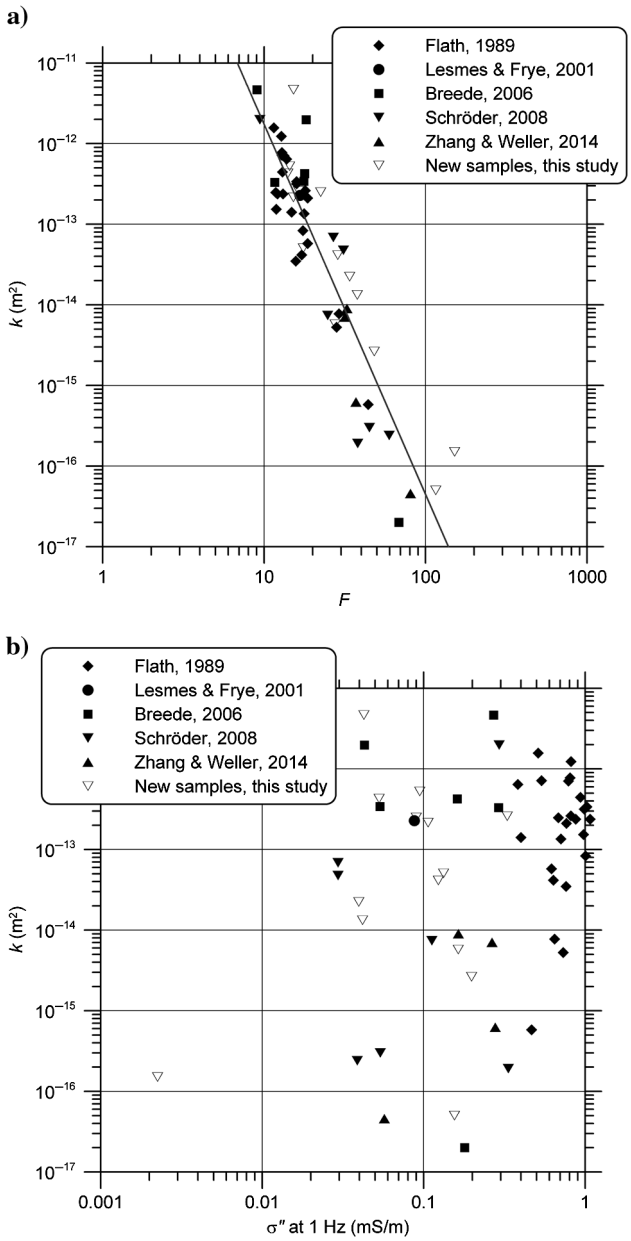

Figure 1. Relationships between permeability and (a) formation factor ($R^2 = 0.832$) and (b) imaginary conductivity for the 56 sandstone samples.

RESULTS

Sandstone samples

The relationships between the (1) formation factor and permeability and (2) imaginary conductivity and permeability are the basis of the k prediction equations examined here. These relationships are plotted for all 56 sandstone samples in Figure 1. It is immediately apparent that the formation factor is well correlated with permeability, whereas the imaginary conductivity is not. Using the permeability, the formation factor, and the imaginary part of conductivity of all 56 sandstone samples, the following equation of permeability prediction is determined:

$$k^* = \frac{2.66 \times 10^{-7}}{F^{5.35}\sigma''^{0.66}}, \tag{19}$$

with k^* being given in m^2, F is unitless, and the imaginary part of conductivity σ'' is given in mS/m. The resulting coefficient of determination $R^2 = 0.884$ indicates statistical relevance. The average deviation $d = 0.383$ indicates a deviation between measured and predicted permeability of less than a half order of magnitude or a factor of 2.4. Equation 19 and Figure 1a highlight the importance of an accurate estimation of the formation factor; the large exponent of 5.35 means that relatively small errors in the formation factor will result in large errors in permeability prediction.

The formation factor is rarely available for most practical field applications in hydrogeophysics. We therefore examined the effect of replacing the formation factor by the low-frequency conductivity σ_0 from DD that is related to the apparent formation factor F' and the fluid conductivity σ_w by

$$\sigma_0 = \frac{1}{F'}\sigma_w. \tag{20}$$

Because the fluid conductivity is nearly constant for all samples in our study, the low-frequency conductivity is inversely proportional to the apparent formation factor. The resulting equation reads

$$k^* = \frac{5.11 \times 10^{-21}\sigma_0^{5.18}}{\sigma''^{2.55}}, \tag{21}$$

but $R^2 = 0.411$ and $d = 0.793$ (k^* is given in m^2, σ_0 and σ'' are given in mS/m), indicating a much worse k-prediction. In this case, the DC conductivity (or apparent formation factor F') is obviously unable to replace the true formation factor that must be recorded with high accuracy given the large exponent on F.

The predictive quality is slightly improved over equation 19 if σ'' is replaced by the normalized chargeability m_n from multifrequency data. The resulting equation reads

$$k^* = \frac{8.69 \times 10^{-7}}{F^{5.38} m_n^{0.79}}, \tag{22}$$

with $R^2 = 0.887$ and $d = 0.374$ (k^* given in m^2, F is unitless, and m_n is given in mS/m). Figure 2 plots the measured permeability versus the predicted permeability according to equations 19 and 22. The diagonal line corresponds to an optimal agreement between measured and predicted values. A shorter distance of the data points from the diagonal indicates a better quality of the permeability estimate. The two dashed lines on either side of the diagonal indicate a deviation of one order of magnitude or a factor of 10 from the measured permeability value. The order of magnitude or better predictions of permeability are valuable given that permeability may readily vary over many orders of magnitude over spatial scales that control fluid flow and transport in natural systems. The 56 sandstone samples are located between or close to the dashed lines. The comparison between equations 19 and 22 indicates only marginal changes when the multifrequency polarization parameter (m_n) is used.

Unconsolidated materials

The set of unconsolidated materials includes complex conductivity, the formation factor, and permeability data from four studies with a total of 22 samples that were saturated with a sodium chloride brine with $\sigma_w \approx 100$ mS/m. This data set was used to explore different equations for permeability prediction based on the generic form presented in equation 15. The best predictive quality was achieved using the formation factor and imaginary part of conductivity. The relationships between the (1) formation factor and permeability and (2) imaginary conductivity and permeability are plotted for the extended set of unconsolidated samples in Figure 3. It is immediately apparent that the imaginary conductivity is well correlated with permeability, whereas the formation factor is not. This result is in direct contrast to that reported for the sandstone samples above. The resulting fitting equation

$$k^* = \frac{1.08 \times 10^{-13}}{F^{1.12} \sigma''^{2.27}} \tag{23}$$

is characterized by a coefficient of determination of $R^2 = 0.862$ and an average absolute deviation of $d = 0.386$ (k^* given in m^2, F is unitless, and σ'' is given in mS/m). Figure 4a shows the comparison between measured and predicted permeability. The predictive quality is nearly the same if σ'' is replaced by the normalized chargeability m_n (Figure 4b). Using the low-frequency conductivity σ_0 in place of the formation factor, the multivariate fitting of the data set consisting of 22 unconsolidated samples results in the following equation:

$$k^* = \frac{3.47 \times 10^{-16} \sigma_0^{1.11}}{\sigma''^{2.41}}, \tag{24}$$

with $R^2 = 0.857$ and $d = 0.414$ (k^* is given in m^2 and σ_0 and σ'' are given in mS/m). Unlike for the sandstone samples, the exponent of the low-frequency conductivity is statistically identical to the exponent of F in equation 23, and the prediction quality is only slightly lower. This behavior is expected given the low sensitivity of k prediction for unconsolidated samples to F in contrast to the corresponding high sensitivity for sandstone samples (factor c is approximately one for the unconsolidated samples compared with five for the sandstones).

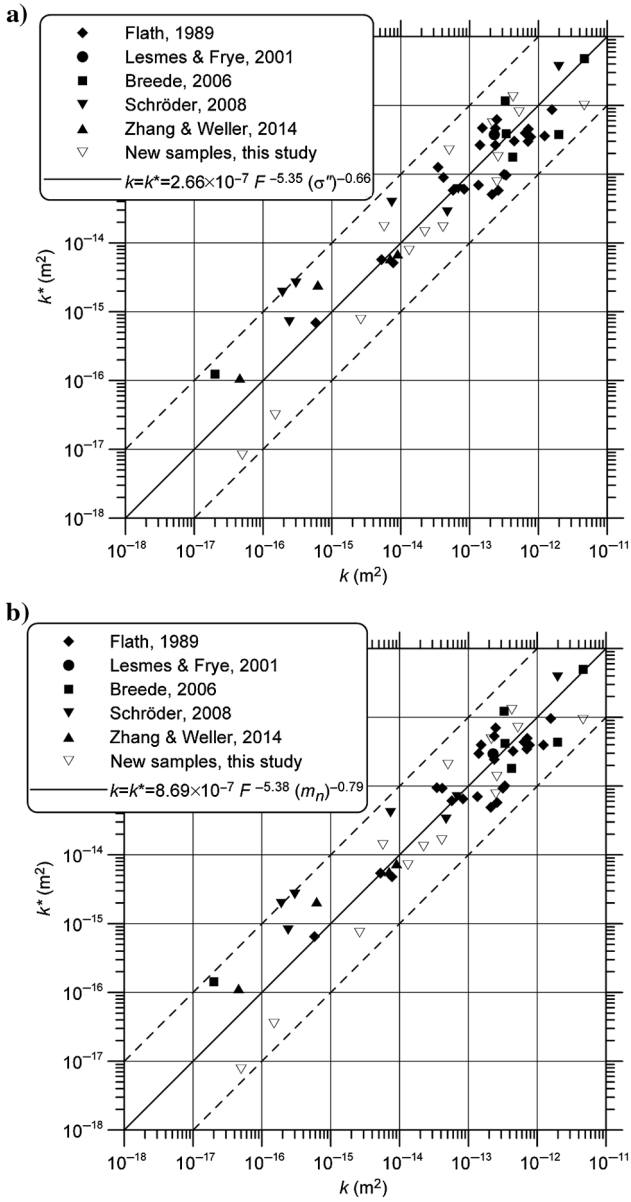

Figure 2. Permeability calculated (a) from equation 19 ($R^2 = 0.884$) and (b) from equation 22 ($R^2 = 0.887$) plotted versus measured permeability for 56 sandstone samples. The two dashed lines on either side of the diagonal indicate a deviation of one order of magnitude from the measured permeability value.

We applied equation 24 to the three additional sample sets that were not considered by the multiple regression fitting procedure because they did not satisfy our stringent requirements regarding the saturating fluid. Figure 5 presents the comparison between measured and predicted permeability determined by equation 24 for the 22 unconsolidated samples and the samples of the three additional sample sets after the necessary corrections. Although the 16 additional samples were not integrated into the fitting procedure, all data points are located inside the two dashed lines and indicate a predictive accuracy within one order of magnitude.

Sandstones and unconsolidated material

A further test was performed to consider permeability prediction for the combined data set of sandstones and unconsolidated materials. The best fitting equation for 91 samples was achieved using the formation factor and the normalized chargeability with

$$k^* = \frac{4.03 \times 10^{-9}}{F^{3.68} m_n^{1.19}}, \tag{25}$$

with k^* given in m^2, F is unitless, and m_n is given in mS/m. The coefficient of determination of $R^2 = 0.716$ is lower than for the separate fitting of sandstones and unconsolidated samples. Figure 6 presents the comparison between measured and predicted per-

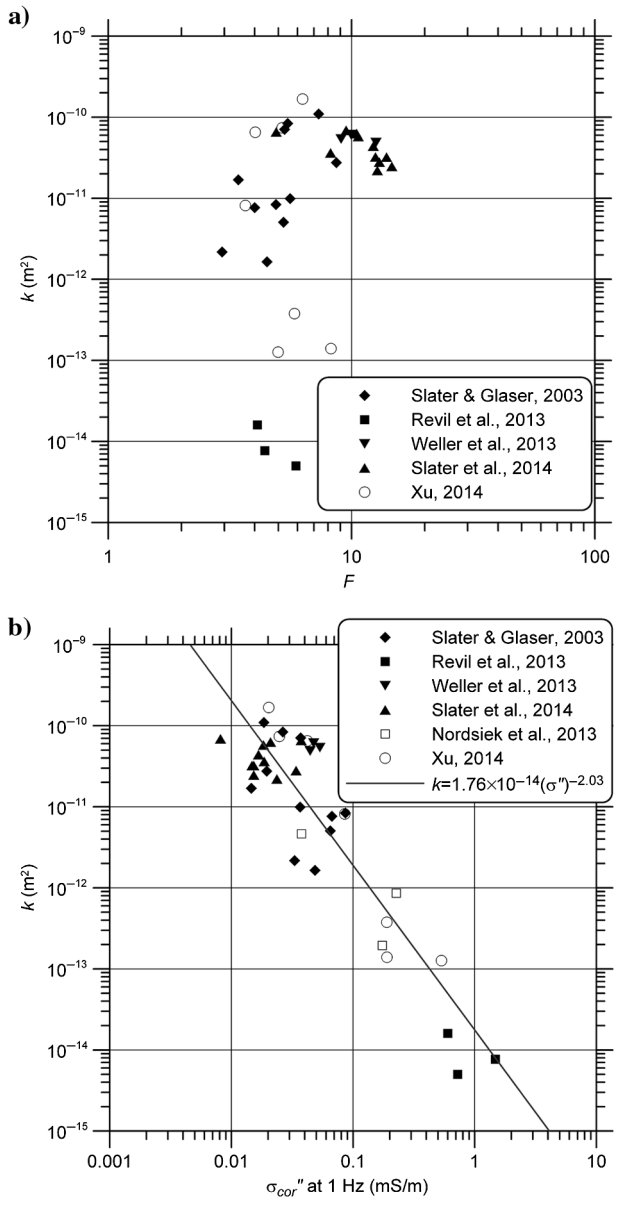

Figure 3. Relationships between permeability and (a) formation factor (for 35 unconsolidated samples) and (b) imaginary conductivity (for 38 unconsolidated samples, $R^2 = 0.813$).

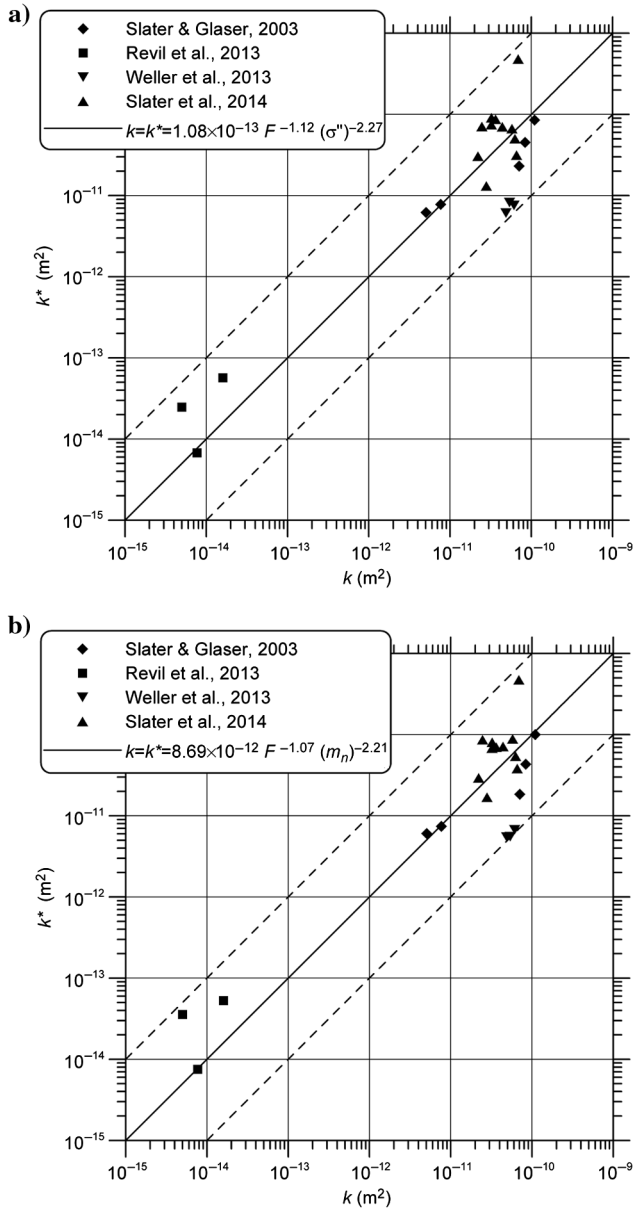

Figure 4. Permeability calculated (a) from the formation factor and imaginary conductivity (equation 23, $R^2 = 0.862$) and (b) from the formation factor and normalized chargeability, plotted versus measured permeability for 22 unconsolidated samples ($R^2 = 0.844$). The two dashed lines on either side of the diagonal indicate a deviation of one order of magnitude from the measured permeability value.

meability determined by equation 25 for the 56 sandstone samples and the 35 samples of unconsolidated material. Sixty-nine of the 91 samples are located between the two dashed lines. A strong deviation with $d > 2$ is observed for four unconsolidated samples.

DISCUSSION

Previous studies have clearly shown that parameters derived from IP measurements can be integrated into models of permeability prediction. However, the existing power law models indicate a considerable variation in the exponents. Most of the previous studies were based on a relatively limited variation in permeability for a specific sample type. We compiled a database from different sources to extend the range of permeability to cover seven orders of magnitude. Equation 15 defines a general form of all such models for permeability prediction using IP data. A multiple regression procedure was applied to determine the factor a and the exponents b and c using different electric parameters available. The resulting exponent b related to the formation factor F indicates values close to five for the set of sandstone samples. This value is also determined by Rink and Schopper (1974) for a large database of sandstone samples in which IP data were unavailable. The exponent $c < 1$ related to the polarization parameters σ'' and m_n in equations 19 and 22 is inconsistent with existing empirical and mechanistic models, where a value $c > 2$ would have been expected. Considering the exponent as a weighting term, the formation factor F is more important for permeability prediction for sandstones than the polarization parameters σ'' and m_n. As a consequence, a high-accuracy measurement of the formation factor F is a necessary precondition for reliable permeability estimation in sandstones. The dominance of the formation factor in determining the permeability of the sandstone samples is illustrated by testing a permeability prediction that ignores IP parameters and is based on the formation factor alone

$$k^* = \frac{6.77 \times 10^{-8}}{F^{4.591}}, \tag{26}$$

with k^* given in m^2 and F is unitless. The resulting coefficient of determination is $R^2 = 0.832$, being only slightly lower than in the case of equations 19 and 22. The average absolute log deviation increases slightly to $d = 0.437$. These small changes in the predictive quality clearly indicate that the formation factor is the most relevant parameter for permeability prediction of sandstones.

The models derived for the unconsolidated samples (based on equation 15) show significantly smaller exponents b for the formation factor F. However, the exponent c on the polarization parameters increases. This is partly a consequence of the smaller variation in the formation factor (from 4 to 15) for the unconsolidated samples. The formation factor F can be replaced by the low-frequency conductivity σ_0 without any appreciable loss in predictive quality. The weak influence of F on permeability in unconsolidated sediments resulted in Slater and Lesmes (2002) reporting a prediction equation based on the imaginary conductivity alone. Following this logic, we derive from our set of 22 unconsolidated samples the following relation between permeability and imaginary part of conductivity:

$$k^* = \frac{2.13 \times 10^{-14}}{\sigma''^{2.04}}, \tag{27}$$

with k^* being given in m^2 and σ'' is given in mS/m. The coefficient of determination is with $R^2 = 0.847$ in the same range as in equations 23 and 24. The average log deviation only slightly increases to

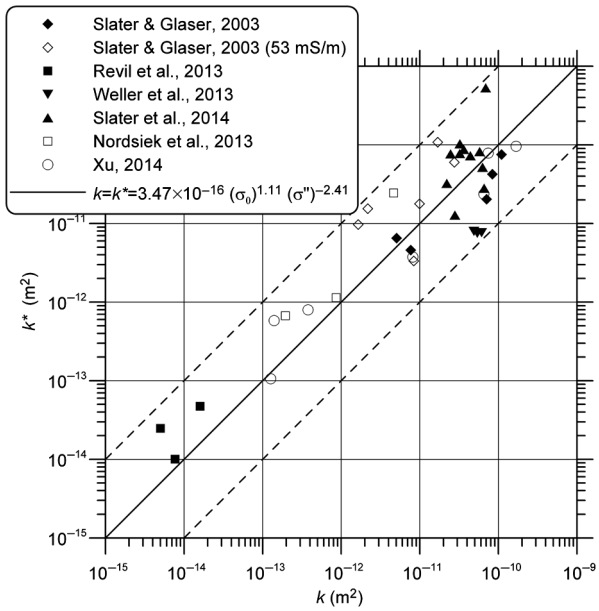

Figure 5. Permeability calculated from equation 24 plotted versus the measured permeability for 38 unconsolidated samples. The full symbols represent the 22 samples that were used to derive equation 24 with a coefficient of determination of $R^2 = 0.857$. The open symbols indicate the additional samples with deviations in fluid conductivity and chemistry after appropriate correction. The two dashed lines on either side of the diagonal indicate a deviation of one order of magnitude from the measured permeability value.

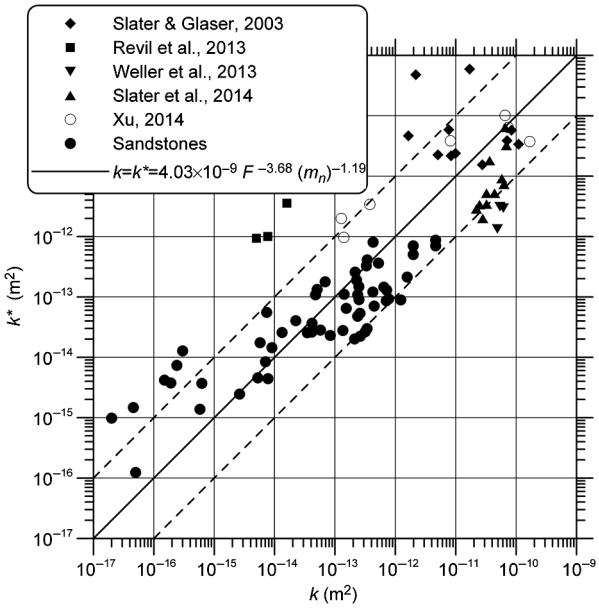

Figure 6. Permeability calculated from equation 25 plotted versus measured permeability for 56 sandstone samples and 35 unconsolidated samples ($R^2 = 0.716$). The two dashed lines on either side of the diagonal indicate a deviation of one order of magnitude from the measured permeability value.

$d = 0.434$. Clearly, the imaginary part of conductivity is the most important parameter for permeability prediction of unconsolidated material. In this study, the imaginary part of conductivity is related to full saturation with a NaCl solution with a fluid conductivity of approximately 100 mS/m. Deviations in fluid conductivity and chemistry have to be corrected accordingly.

Although we have demonstrated that the models for permeability prediction vary considerably between sandstones and unconsolidated materials, a fitting was still made with the complete data set. The resulting equation 25 presents a compromise in fitting the set of sandstone samples (formation factor controlled) and the set of unconsolidated material (imaginary conductivity controlled). The resulting exponent $b = 3.68$ is smaller than that for the sandstones and larger than that for the unconsolidated material. The larger b exponent partly results from the bias due to the greater number of sandstone samples (56) versus unconsolidated samples (35). The larger weight of the sandstone samples leads to some overestimation of permeability for some unconsolidated samples. Regarding the considerable number of samples with a permeability prediction outside the order of magnitude limit, equation 25 does not provide a reliable approach to prediction of the permeability of unknown material.

This study demonstrates that it will not be possible to design a universal model of permeability prediction including only two geoelectric parameters. We acknowledge that different models are based on specific assumptions that are not fulfilled for all materials. Other parameters beyond those related to the pore size distribution are required to reliably predict permeability over the widest possible range of samples. The roughness of the internal surface, the clay content, and the connectivity of the pore space affect the permeability.

CONCLUSIONS

We have demonstrated that permeability prediction based on electric proxy measures of porosity and pore-normalized surface area has potential over a wide range (seven orders of magnitude) of permeability variation. However, the relative importance of the proxy porosity term versus the proxy surface area term is very different for sandstones versus unconsolidated sediments. In sandstone, it is the proxy measure of effective porosity (formation factor or real part of electric conductivity used here) that exerts the dominant control on the permeability. This presents substantial challenges for the field-scale prediction of permeability from electric measurements because accurate estimation of the formation factor requires multisalinity measurements or measurements at high salinities outside of the natural range of potable groundwater, so that the effects of surface conduction can be ignored. Neither of these approaches are typically practical in borehole logging or surface-based applications of geophysical techniques. In contrast, it is the proxy measure of the surface area (imaginary conductivity or normalized chargeability used here) that is most important for k prediction in unconsolidated sediments. These measurements are readily obtainable from IP measurements in the field, although correction factors for variations in fluid chemistry may be required e.g., for Na- versus Ca-dominated groundwater. Consequently, reliable field-scale estimation of permeability from electric measurements is likely more readily achievable for unconsolidated sediments than for sandstones. Our findings highlight the value of empirical investigations using databases spanning the widest possible range of physical parameters for gaining better insight into the opportunity to estimate k from electric geophysical measurements.

ACKNOWLEDGMENTS

We are particularly grateful to D. Flath for providing access to her thesis and data sets. We also thank K. Breede, E. Diamantopoulos, D. Grunat, H. Schröder, and Z. Zhang for data sets.

REFERENCES

Attwa, M., and T. Günther, 2013, Spectral induced polarization measurements for predicting the hydraulic conductivity in sandy aquifers: Hydrology and Earth Systems Sciences, **17**, 4079–4094, doi: 10.5194/hess-17-4079-2013.

Binley, A., L. Slater, M. Fukes, and G. Cassiani, 2005, The relationship between frequency dependent electrical conductivity and hydraulic properties of saturated and unsaturated sandstone: Water Resources Research, **41**, W12417, doi: 10.1029/2005WR004202.

Börner, F. D., and J. H. Schön, 1991, A relation between the quadrature component of electrical conductivity and the specific surface area of sedimentary rocks: Log Analyst, **32**, 612–613.

Börner, F. D., J. R. Schopper, and A. Weller, 1996, Evaluation of transport and storage properties in the soil and groundwater zone from induced polarization measurements: Geophysical Prospecting, **44**, 583–601, doi: 10.1111/j.1365-2478.1996.tb00167.x.

Breede, K., 2006, SIP-Messungen an Sandsteinen: Unpublished diploma thesis, Technische Universität Clausthal.

Flath, D., 1989, The low-frequency complex electrical response of brine-saturated shaly sandstones: Ph.D. thesis, University of Birmingham.

Frohlich, R. K., J. J. Fisher, and E. Summerly, 1996, Electric-hydraulic conductivity correlation in fractured crystalline bedrock: Central Landfill, Rhode Island, USA: Journal of Applied Geophysics, **35**, 249–259, doi: 10.1016/0926-9851(96)00028-6.

Guéguen, Y., and V. Palciauskas, 1994, Introduction to the physics of rocks: Princeton University Press.

Heigold, P. C., R. H. Gilkeson, K. Cartwright, and P. C. Reed, 1979, Aquifer transmissivity from surficial electrical methods: Ground Water, **17**, 338–345, doi: 10.1111/j.1745-6584.1979.tb03326.x.

Hördt, A., A. Druiventak, R. Blaschek, F. Binot, A. Kemna, P. Kreye, and N. Zisser, 2009, Case histories of hydraulic conductivity estimation with induced polarization at the field scale: Near Surface Geophysics, **7**, 529–545, doi: 10.3997/1873-0604.2009035.

Johnson, D. L., J. Koplik, and L. Schwartz, 1986, New pore-size parameter characterizing transport in porous media: Physical Review Letters, **57**, 2564–2567, doi: 10.1103/PhysRevLett.57.2564.

Kelly, W. E., 1977, Geoelectric sounding for estimating aquifer hydraulic conductivity: Ground Water, **15**, 420–425, doi: 10.1111/j.1745-6584.1977.tb03189.x.

Kelly, W. E., and P. E. Reiter, 1984, Influence of anisotropy on relations between aquifer hydraulic and electrical properties: Journal of Hydrology, **74**, 311–321, doi: 10.1016/0022-1694(84)90021-0.

Kosinski, W. K., and W. E. Kelly, 1981, Geoelectric soundings for predicting aquifer properties: Ground Water, **19**, 163–171, doi: 10.1111/j.1745-6584.1981.tb03455.x.

Lesmes, D. P., and K. M. Frye, 2001, Influence of pore fluid chemistry on the complex conductivity and induced polarization responses of Berea sandstone: Journal of Geophysical Research, **106**, 4079–4090, doi: 10.1029/2000JB900392.

Lesmes, D. P., and F. D. Morgan, 2001, Dielectric spectroscopy of sedimentary rocks: Journal of Geophysical Research, **106**, 13329–13346, doi: 10.1029/2000JB900402.

Mazac, O., and I. Landa, 1979, On determination of hydraulic conductivity and transmissivity of aquifers by vertical electric sounding: Journal of Geological Science, **16**, 123–129.

Nordsiek, S., A. Hördt, E. Diamantopoulos, and W. Durner, 2013, Estimation of van Genuchten-Mualem parameters from spectral induced polarization measurements: Presented at Near Surface Geoscience Conference.

Nordsiek, S., and A. Weller, 2008, A new approach to fitting induced-polarization spectra: Geophysics, **73**, no. 6, F235–F245, doi: 10.1190/1.2987412.

Pape, H., L. Riepe, and J. R. Schopper, 1987, Theory of self-similar network structures in sedimentary and igneous rocks and their investigation with microscopical methods: Journal of Microscopy, **148**, 121–147, doi: 10.1111/j.1365-2818.1987.tb02861.x.

Ponzini, G., A. Ostroman, and M. Molinari, 1983, Empirical relation between electrical transverse resistance and hydraulic transmissivity: Geoexploration, **22**, 1–15, doi: 10.1016/0016-7142(84)90002-4.

Purvance, D. T., and R. Andricevic, 2000, Geoelectric characterization of the hydraulic conductivity field and its spatial structure at variable scales: Water Resources Research, **36**, 2915–2924, doi: 10.1029/2000WR900187.
Revil, A., 2012, Induced polarization of shaly sands: Influence of the electrical double layer: Water Resources Research, **48**, W02517.
Revil, A., and N. Florsch, 2010, Determination of permeability from spectral induced polarization in granular media: Geophysical Journal International, **181**, 1480–1498.
Revil, A., N. Florsch, and C. Camerlynck, 2014a, Spectral induced polarization porosimetry: Geophysical Journal International, **198**, 1016–1033, doi: 10.1093/gji/ggu180.
Revil, A., P. Kessouri, and C. Torres-Verdin, 2014b, Electrical conductivity, induced polarization, and permeability of the Fontainebleau sandstone: Geophysics, **79**, no. 5, D301–D318, doi: 10.1190/geo2014-0036.1.
Revil, A., and M. Skold, 2011, Salinity dependence of spectral induced polarization in sands and sandstones: Geophysical Journal International, **187**, 813–824, doi: 10.1111/j.1365-246X.2011.05181.x.
Revil, A., M. Skold, S. S. Hubbard, Y. Wu, D. B. Watson, and M. Karaoulis, 2013, Petrophysical properties of saprolites from the Oak Ridge Integrated Field Research Challenge site, Tennessee: Geophysics, **78**, no. 1, D21–D40, doi: 10.1190/geo2012-0176.1.
Rink, M., and J. R. Schopper, 1974, Interface conductivity and its implication to electric logging: Presented at SPWLA 15th Annual Logging Symposium, Paper J.
Schröder, H., 2008, SIP-Messungen an mit unterschiedlichen Salzlösungen gesättigten Sandsteinen: Diploma thesis, Technische Universität Clausthal.
Sen, P. N., C. Straley, W. E. Kenyon, and M. S. Whittingham, 1990, Surface-to-volume ratio, charge density, nuclear magnetic relaxation, and permeability in clay-bearing sandstones: Geophysics, **55**, 61–69, doi: 10.1190/1.1442772.
Slater, L., 2007, Near surface electrical characterization of hydraulic conductivity: From petrophysical properties to aquifer geometries — A review: Surveys in Geophysics, **28**, 169–197.
Slater, L., W. Barrash, J. Montrey, and A. Binley, 2014, Electrical-hydraulic relationships observed for unconsolidated sediments in the presence of a cobble framework: Water Resources Research, **50**, 5721–5742, doi: 10.1002/2013WR014631.
Slater, L., and D. P. Lesmes, 2002, Electrical-hydraulic relationships observed for unconsolidated sediments: Water Resources Research, **38**, 1213, doi: 10.1029/2001WR001075.
Slater, L. D., and D. R. Glaser, 2003, Controls on induced polarization in sandy unconsolidated sediments and application to aquifer characterization: Geophysics, **68**, 1547–1558, doi: 10.1190/1.1620628.
Sumner, J. S., 1976, Principles of induced polarization for geophysical exploration: Elsevier.
Urish, D., 1981, Electrical resistivity-hydraulic conductivity relationships in glacial outwash aquifers: Water Resources Research, **17**, 1401–1408, doi: 10.1029/WR017i005p01401.
Vinegar, H. J., and M. H. Waxman, 1984, Induced polarization of shaly sands: Geophysics, **49**, 1267–1287, doi: 10.1190/1.1441755.
Waxman, M. H., and L. J. M. Smits, 1968, Electrical conductivities in oil-bearing shaly sands: Transactions of the American Institute of Mining and Metallurgical Engineers, **243**, 107–122.
Weller, A., K. Breede, L. Slater, and S. Nordsiek, 2011, Effect of changing water salinity on complex conductivity spectra of sandstones: Geophysics, **76**, no. 5, F315–F327, doi: 10.1190/geo2011-0072.1.
Weller, A., M. A. Kassab, W. Debschütz, and C.-D. Sattler, 2014, Permeability prediction of four Egyptian sandstone formations: Arabian Journal of Geosciences, **7**, 5171–5183, doi: 10.1007/s12517-013-1188-7.
Weller, A., S. Nordsiek, and W. Debschütz, 2010a, Estimating permeability of sandstone samples by nuclear magnetic resonance and spectral-induced polarization: Geophysics, **75**, no. 6, E215–E226, doi: 10.1190/1.3507304.
Weller, A., L. Slater, S. Nordsiek, and D. Ntarlagiannis, 2010b, On the estimation of specific surface per unit pore volume from induced polarization: A robust empirical relation fits multiple data sets: Geophysics, **75**, no. 4, WA105–WA112, doi: 10.1190/1.3471577.
Weller, A., L. Slater, and S. Nordsiek, 2013, On the relationship between induced polarization and surface conductivity: Implications for petrophysical interpretation of electrical measurements: Geophysics, **78**, no. 5, D315–D325, doi: 10.1190/geo2013-0076.1.
Weller, A., and L. Slater, 2012, Salinity dependence of complex conductivity of unconsolidated and consolidated materials: Comparisons with electrical double layer models: Geophysics, **77**, no. 5, D185–D198, doi: 10.1190/geo2012-0030.1.
Xu, S., 2014, Hydraulic conductivity estimation through complex electrical conductivity in unconsolidated soil: M.S. thesis, Lancaster University.
Zhang, Z., and A. Weller, 2014, Fractal dimension of pore space geometry of an Eocene sandstone formation: Geophysics, **79**, no. 6, D377–D387, doi: 10.1190/geo2014-0143.1.
Zisser, N., A. Kemna, and G. Nover, 2010, Relationship between low-frequency electrical properties and hydraulic permeability of low-permeability sandstones: Geophysics, **75**, no. 3, E131–E141, doi: 10.1190/1.3413260.